AIAA JOURNAL
Vol. 40, No. 5, May 2002

Schemes to Compute Unsteady Flashing Flows

Michel Barret*
Institut Universitaire de Technologie Sénart, 77127 Lieusaint, France
Eric Faucher†
Electricite de France, 77250 Moret-Sur-Loing, France
and
Jean-Marc Hérard‡
Electricite de France, 78400 Chatou, France

Some ways to compute flashing flows in variable cross section ducts are provided, focusing on the homogeneous relaxation model. The basic numerical method relies on a splitting technique that is consistent with the overall entropy inequality. The cross section is assumed to be continuous, and the finite volume approach is applied to approximate homogeneous equations. Several suitable schemes to account for complex equation of state are discussed, namely, the Rusanov scheme, an approximate form of the Roe scheme, and the "volumes finis Roe" (VFRoe) scheme with the help of nonconservative variables. To evaluate respective accuracy, the homogeneous Euler equations are computed first, and the L1 error norm of transient solutions of shock tube experiments are plotted. It is shown that the Rusanov scheme is indeed less accurate, which balances its interesting properties, inasmuch as it preserves the positivity of the mean density and the maximum principle for the vapor quality. Computations of real cases are presented, which account for the mass transfer term and the time–space dependent cross sections.

I. Introduction

SOME applications in industry require predicting flashing flows in variable cross section ducts. In some cases, it even becomes compulsory to account for cross sections that also vary in time, for instance, when predicting flows in safety valves, which was one of the basic motivations of the following developments. From the modeling point of view, it is virtually acknowledged that the homogeneous relaxation model is accurate enough to represent the true behavior of that kind of flow. In past years, Bolle et al.,[1] Bilicki and Kardas,[2] Bilicki et al.,[3] and Downar-Zapolski et al.[4] investigated such closures. For stationary one-dimensional flows, this model enables the prediction of the critical mass flow rate and the pressure distribution with a good accuracy.[1–4] It requires some timescale to account for mass transfer, which governs phase change in strong rarefaction waves. Friction effects will be disregarded herein, though they may be easily accounted for without altering the global behavior of the algorithm. This is because the mean diameter of pipes in our applications is rather large. The present contribution actually aims at providing some ways to compute these complex industrial problems involving unsteady flashing flows and, more specifically, at providing deep insight on the strength and weaknesses of three different upwinding techniques used in finite volume conservative schemes. Emphasis is given to the latter schemes because they allow computation of any equation of state (EOS) on any kind of mesh.

Received 26 July 2000; revision received 19 July 2001; accepted for publication 27 August 2001.

*Associate Professor, Laboratoire Thermique et Mécanique des Fluides, Avenue Pierre Point; barret@univ-paris12.fr.

†Ph.D. Student, Division Recherche Développement, Département Mécanique et Technologie des Composants, Centre des Renardières; also Ph.D. Student, Laboratoire Thermique et Mécanique des Fluides, Institut Universitaire de Technologie Sénart, Avenue Pierre Point, 77127 Lieusaint, France.

‡Senior Engineer, Division Recherche Développement, Département Mécanique des Fluides et Transferts Thermiques, 6, quai Watier; Jean-Marc.Herard@der.edf.fr; also Associate Research Director, Centre de Mathématique et d'Informatique, Laboratoire Analyse Topologie et Probabilités, UMR Centre National de la Recherche Scientifique 6632, Université de Provence, 39, rue Joliot Curie, 13453 Marseille, France; Herard@cmi.univ-mrs.fr. Member AIAA.

We first describe the basics of the homogeneous relaxation model (HRM), which governs the motion of the two-phase mixture, assuming that relative velocities are small compared with the speed of acoustic waves in the medium and have little influence on the whole behavior of the flashing flows. Then, the overall numerical technique of Ref. 5 is briefly recalled, which relies on the finite volume method.[6] Special emphasis is given to three upwinding schemes to account for convective fluxes: an approximate Godunov[7] scheme (see Refs. 8–14 based on the initial proposition of Refs. 15 and 16) and extended versions of Rusanov[17] and Roe[18] schemes (also see Ref. 19) to the frame of nonconservative systems[20–23] (see Refs. 24 and 25 for the theoretical framework). Some properties of the schemes are recalled, and special emphasis is given on the true level accuracy (and the rate of convergence) obtained with the three schemes, focusing on either steady flows in nozzles or on shock tube experiments involving gas, vapor, or liquid and complex EOS. More precisely, the L1 error norm is plotted in various cases, which provides quantitative comparison that is seldomly available in the literature. This is one of the main contributions of the present work, which examines both steady and highly unsteady flow patterns. Eventually, we present an application of some two-phase flashing flow in a nozzle; this case is examined using the three different schemes. Although important in practice, considerations about parallelizing of the code are not discussed herein, and the reader is referred to Refs. 26 and 27 for this subject matter. Appendices A–D provide more information on the way boundary conditions are handled[28] and on the efficient "volumes finis Roe" (VFRoe)-nonconservative variable (NCV) approximate Godunov scheme.[8–12]

II. Basic Set of Equations

The basic set of equations of the HRM consists of the following four equations, which govern the conservation laws for mass of the two-phase mixture, vapor phase, and total energy of both phases and an additional nonconservative equation for the mean momentum[1–4,29–31]:

$$
\begin{aligned}
&[\rho S(x,t)\alpha]_{,t} + [\rho S(x,t)U\alpha]_{,x} = S(x,t)\Gamma \\
&[\rho S(x,t)]_{,t} + [\rho S(x,t)U]_{,x} = 0 \\
&[\rho S(x,t)U]_{,t} + [\rho S(x,t)U^2]_{,x} + S(x,t)P_{,x} = 0 \\
&[S(x,t)E]_{,t} + [S(x,t)(E+P)U]_{,x} + P[S(x,t)]_{,t} = 0
\end{aligned} \qquad (1)
$$

when restricted to adiabatic flows. $S(x,t)$ is the mean continuous cross section (otherwise, previous equations are meaningless) and is expected to be provided by users. Here, ρ, U, P, α, and E are the mean density, the mean velocity, the mean pressure, the vapor quality (which is expected to lie in [0,1]), and the mean total energy of the two-phase mixture in the mean section, respectively. Subscripts t and x denote the time and space variables. The total energy of the two-phase mixture is related to the internal energy as follows:

$$E = \rho e(\tau, \alpha, P) + \tfrac{1}{2}\rho u^2 \tag{2}$$

where τ is the specific volume ($\tau = 1/\rho$). This must be supplemented by closure laws for the mass transfer term Γ and for the total internal energy of the two-phase mixture e, which is given by

$$e(\tau, \alpha, P) = \alpha\, e_{\mathrm{SV}}(P) + (1-\alpha)\, e_{\mathrm{ML}}\left[P, \frac{\tau - \alpha\tau_{\mathrm{SV}}(P)}{1-\alpha}\right] \tag{3}$$

Metastable liquid (ML) and saturated vapor (SV) are indicated by subscripts. Thermodynamic laws are given by Pollack.[32]

An important issue when computing flashing flows concerns the forms for the mass transfer term. A simplified form for this term was proposed in Refs. 1–4:

$$\Gamma = -\rho[(\alpha - \bar{\alpha})/\theta] \tag{4}$$

The mass transfer term requires computing the equilibrium quality:

$$\bar{\alpha} = \frac{h - h_{\mathrm{SL}}(P)}{h_{\mathrm{SV}}(P) - h_{\mathrm{SL}}(P)} \tag{5}$$

where $h_{\mathrm{SL}}(P)$ and $h_{\mathrm{SV}}(P)$, respectively, denote the specific enthalpy of the saturated liquid (SL) and the SV. Correlations used in computations for the timescale θ were given by Downar Zapolski et al.[4] and are recalled in Appendix C.

Before focusing on the numerical implementation of the model, we need to introduce some additional variables. Throughout the paper

$$\hat{\gamma} = \frac{1}{(\partial e/\partial P)_{\tau,\alpha}}\left[\tau + \frac{\tau}{P}\left(\frac{\partial e}{\partial \tau}\right)_{P,\alpha}\right] \tag{6}$$

and the square of the celerity of density waves is $c^2 = \hat{\gamma} P \tau$. The specific entropy, $s = s(P, \tau, \alpha)$, is a function in agreement with

$$\hat{\gamma} P\left(\frac{\partial s}{\partial P}\right)_{\tau,\alpha} - \tau\left(\frac{\partial s}{\partial \tau}\right)_{P,\alpha} = 0 \tag{7}$$

Hence, the whole model is closed.

III. Numerical Method

The numerical method is based on a fractional step technique,[21,33] which allows computing time variations of the mean cross section and the remaining of convective and source terms. The overall technique is detailed in Ref. 5. It is shown there that the splitting technique is in agreement with the whole entropy inequality. Moreover, the computation of the partial differential equations in frozen duct (with respect to time) still may be split into two steps: The first one involves the computation of the mass transfer term, and the second one deals with the homogeneous nonconservative convective effects.[24,25] Because of the ratio of the timescale associated with the fast acoustic waves over the timescale θ, which is smaller than one in practice, the fractional step approach is not penalized as may occur when computing other systems. In Ref. 5, it is shown that the specific form of the mass transfer term enables ensuring the maximum principle for the vapor quality for regular enough solutions. Details on numerical implementation of boundary conditions can be found in Appendix B (also see Refs. 28 and 29 for further details). Thus, we only focus here on the comparison between three different ways to deal with convective terms. Alternative ways to deal with source terms, including a comparison with techniques suggested in Ref. 34 can be found in Ref. 29.

The main two steps follow. Given some time step Δt^n and initial data $\boldsymbol{W}^n$ at time t^n, one computes the following ordinary differential equation for given mean values of $\boldsymbol{W}_i^n$ over cell i:

$$\boldsymbol{W}_i^n = \int_{\Omega_i} \boldsymbol{W}(x, t^n)\frac{\mathrm{d}x}{h_i}$$

The time step is chosen in agreement with some Courant–Friedrichs–Lewy (CFL) condition, and h_i is the mesh size of cell i.

Step 1:

$$[\rho S(x,t)\alpha]_{,t} = S(x,t)\Gamma, \qquad [\rho S(x,t)]_{,t} = 0$$

$$[\rho S(x,t)U]_{,t} = 0, \qquad [S(x,t)E]_{,t} + P[S(x,t)]_{,t} = 0$$

$$[S(x,t)]_{,t} = j(x,t) \tag{8}$$

provides that on each cell i of the mesh

$$\tilde{\boldsymbol{W}}_i = \psi_1\left(\left\{\boldsymbol{W}_k^n\right\}_{k\in Z}\right)$$

Obviously, this step is skipped when the cross section does not vary with time [$j(x,t) = 0$]. We recall that the mean velocity and the specific entropy do not vary through this step. The vapor quality and the mean density agree with

$$\alpha_{,t} = \Gamma/\rho, \qquad (\log\rho)_{,t} = -j/S$$

Once step 1 is solved, the convective system is solved over the time interval $[t^n, t^n + \Delta t^n]$, given initial data $\tilde{\boldsymbol{W}}_i^n$ on each cell and suitable boundary conditions.

Step 2:

$$[\rho S(x,t)\alpha]_{,t} + [\rho S(x,t)\alpha U]_{,x} = 0$$

$$[\rho S(x,t)]_{,t} + [\rho S(x,t)U]_{,x} = 0$$

$$[\rho S(x,t)U]_{,t} + [\rho S(x,t)U^2]_{,x} + S(x,t)P_{,x} = 0$$

$$[S(x,t)E]_{,t} + [S(x,t)(E+P)U]_{,x} = 0, \qquad [S(x,t)]_{,t} = 0 \tag{9}$$

provides that on each cell i of the mesh

$$\boldsymbol{W}_i^{n+1} = \psi_2\left(\{\tilde{\boldsymbol{W}}_k\}_{k\in Z}\right)$$

Details pertaining to Riemann invariants of the homogeneous part of step 2, on shock relations, and on positivity constraints through the one-dimensional Riemann problem (see Ref. 35) associated with the latter system are recalled in a previous paper.[5] The source term may be computed with an extra fractional step method. This may be done in the simplest following way (which preserves the maximum principle for the vapor quality at a discrete level), by computing $\alpha(t + \Delta t)$ as a function of $\alpha(t)$ as

$$\alpha(t+\Delta t) = \exp[-\Delta t/\theta(t)]\alpha(t) + \{1 - \exp[-\Delta t/\theta(t)]\}\bar{\alpha}(t) \tag{10}$$

or by using interface values of state variables. We now discuss upwinding techniques.[36]

IV. Upwinding Techniques

We will now focus on the computation of the convective system (step 2) using three different schemes; the three schemes enable handling complex thermodynamic laws. The convective system (9) may be written in condensed form as

$$(S\boldsymbol{W})_{,t} + [S\boldsymbol{F}(\boldsymbol{W})]_{,x} + S\boldsymbol{G}(\boldsymbol{W})_{,x} = \boldsymbol{0} \tag{11}$$

where $\boldsymbol{W}$ is the physical convervative variable. The flux functions are given by

$$\boldsymbol{F}(\boldsymbol{W})^t = [\rho U\alpha, \rho U, \rho U^2, U(E+P)] \tag{12a}$$

$$\boldsymbol{G}(\boldsymbol{W})^t = (0, 0, P, 0) \tag{12b}$$

The basic idea follows. The given section of the duct is discretized and is assumed to be piecewise linear on each interface of control volumes. Also, we introduce constant reconstruction of the conservative variable

$$\boldsymbol{W}^t = (\rho\alpha, \rho, \rho U, E) \tag{13}$$

over cell i (Fig. 1).

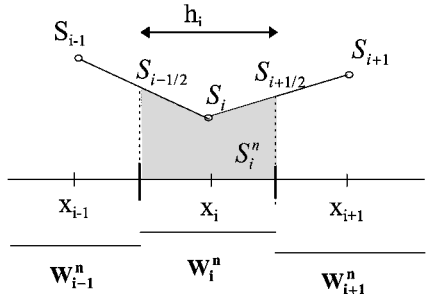

Fig. 1 Sketch of the mesh.

Given some approximate values of the cross section at the cell center S at time t^n, the cross section at the interface is defined using a linear interpolation:

$$S_{i+\frac{1}{2}} = \frac{h_i S_{i+1} + h_{i+1} S_i}{h_i + h_{i+1}} \tag{14}$$

The mean value of $S(x)$ over cell Ω_i is given by

$$\widehat{S}_i = \int_{\Omega_i} S(x, t^n) \frac{\mathrm{d}x}{h_i} \tag{15a}$$

or

$$\widehat{S}_i = S_i \left[1 - \frac{h_i}{4(h_i + h_{i+1})} - \frac{h_i}{4(h_i + h_{i-1})} \right] + \frac{h_i}{4} \left(\frac{S_{i-1}}{h_i + h_{i-1}} + \frac{S_{i+1}}{h_i + h_{i+1}} \right) \tag{15b}$$

All schemes will take the form

$$h_i \widehat{S}_i \left(\boldsymbol{W}_i^{n+1} - \tilde{\boldsymbol{W}}_i \right) + \Delta t^n \widehat{S}_i \left(G_{i+\frac{1}{2}}^{\text{scheme}} - G_{i-\frac{1}{2}}^{\text{scheme}} \right) + \Delta t^n \left\{ S_{i+\frac{1}{2}} \boldsymbol{F}_{i+\frac{1}{2}}^{\text{scheme}} - S_{i-\frac{1}{2}} \boldsymbol{F}_{i-\frac{1}{2}}^{\text{scheme}} \right\} = \boldsymbol{0}$$

We next define various forms of numerical fluxes $\boldsymbol{F}^{\text{scheme}}$ and $\boldsymbol{G}^{\text{scheme}}$. These formulas should provide consistant and stable approximation of fluxes in the sense of Ref. 6. We use the standard notation

$$\bar{\phi}_{i+\frac{1}{2}} = (\phi_i + \phi_{i+1})/2$$

A. Rusanov Scheme

An extension of the original Rusanov scheme[18] yields

$$\left(\boldsymbol{G}_{i+\frac{1}{2}}^{\text{Rusanov}} \right)^t = \left(0, 0, \bar{\tilde{P}}_{i+\frac{1}{2}}, 0 \right) \tag{16}$$

$$\boldsymbol{F}_{i+\frac{1}{2}}^{\text{Rusanov}} (\tilde{\boldsymbol{W}}_i, \tilde{\boldsymbol{W}}_{i+1}) = \tfrac{1}{2} [\boldsymbol{F}(\tilde{\boldsymbol{W}}_i) + \boldsymbol{F}(\tilde{\boldsymbol{W}}_{i+1}) - \bar{s}_{i+\frac{1}{2}} (\tilde{\boldsymbol{W}}_{i+1} - \tilde{\boldsymbol{W}}_i)] \tag{17}$$

where

$$\bar{s}_{i+\frac{1}{2}} = \max(|\tilde{u}_i| + \tilde{c}_i, |\tilde{u}_{i+1}| + \tilde{c}_{i+1}) \tag{18}$$

noting the numerical sound velocity

$$\hat{c}_i^2 = \tilde{\hat{\gamma}}_i \tilde{P}_i \tilde{\tau}_i \tag{19}$$

Recall that one of the main advantages of Rusanov scheme is that it ensures the positivity of the density and the discrete maximum principle for the vapor quality provided that some CFL condition holds (see Appendix A).

B. Approximate Form of Roe Scheme

In a somewhat different framework, an extension of the original Roe scheme[17] to the frame of nonconservative systems was proposed in Ref. 23. This enables one to handle time-dependent and stationary flows. We use here a slightly modified version of the scheme (see also Ref. 20), which does not require consistancy with the integral form of the conservation law, as the standard Roe scheme[17] does, and, thus, is useful when dealing with complex EOS. For convenience, we define

$$\boldsymbol{B}(\boldsymbol{W}) = \frac{\partial \boldsymbol{F}(\boldsymbol{W})}{\partial \boldsymbol{W}} + \frac{\partial \boldsymbol{G}(\boldsymbol{W})}{\partial \boldsymbol{W}} \tag{20}$$

and introduce

$$\boldsymbol{F}_{i+\frac{1}{2}}^{\text{Roe}} (\tilde{\boldsymbol{W}}_i, \tilde{\boldsymbol{W}}_{i+1}) = \tfrac{1}{2} \{ \boldsymbol{F}(\tilde{\boldsymbol{W}}_i) + \boldsymbol{F}(\tilde{\boldsymbol{W}}_{i+1}) - |\boldsymbol{B}[\hat{\boldsymbol{W}}(\tilde{\boldsymbol{Y}}_i, \tilde{\boldsymbol{Y}}_{i+1})]| (\tilde{\boldsymbol{W}}_{i+1} - \tilde{\boldsymbol{W}}_i) \} \tag{21}$$

noting

$$|\boldsymbol{B}[\hat{\boldsymbol{W}}(\tilde{\boldsymbol{Y}}_i, \tilde{\boldsymbol{Y}}_{i+1})]| = \Omega[\hat{\boldsymbol{W}}(\tilde{\boldsymbol{Y}}_i, \tilde{\boldsymbol{Y}}_{i+1})]| \Lambda[\hat{\boldsymbol{W}}(\tilde{\boldsymbol{Y}}_i, \tilde{\boldsymbol{Y}}_{i+1})]| \times \{ \Omega[\hat{\boldsymbol{W}}(\tilde{\boldsymbol{Y}}_i, \tilde{\boldsymbol{Y}}_{i+1})] \}^{-1} \tag{22}$$

$$\boldsymbol{B}(\boldsymbol{W}) = \Omega(\boldsymbol{W}) \Lambda(\boldsymbol{W}) [\Omega(\boldsymbol{W})]^{-1} \tag{23}$$

Matrix $\Omega(\boldsymbol{W})$ represents the matrix of right eigenvectors of matrix $\boldsymbol{B}(\boldsymbol{W})$ introduced in Eq. (20), associated matrix $\Lambda(\boldsymbol{W})$ is the diagonal matrix containing ordered eigenvalues

$$\lambda_1 = U - c, \qquad \lambda_2 = \lambda_3 = U, \qquad \lambda_4 = U + c$$

Eventually $|\Lambda(\widehat{\boldsymbol{W}})|_{kk} = |\lambda_k[\Lambda(\widehat{\boldsymbol{W}})]|$. The mean value of the conservative state is defined as

$$\hat{\boldsymbol{W}}(\tilde{\boldsymbol{Y}}_i, \tilde{\boldsymbol{Y}}_{i+1}) = \boldsymbol{W}[(\tilde{\boldsymbol{Y}}_i + \tilde{\boldsymbol{Y}}_{i+1})/2] \tag{24}$$

where variable Y is defined as $\boldsymbol{Y}^t = (\alpha, \tau, u, P)$. Note that $G_{i+1/2}^{\text{Roe}}$ is still given as

$$\left(G_{i+\frac{1}{2}}^{\text{Roe}} \right)^t = \left(0, 0, \bar{\tilde{P}}_{i+\frac{1}{2}}, 0 \right) \tag{25}$$

This scheme has been extensively used to predict the behavior of second-order turbulent closures in single-phase flows, when no Roe's[17] average is available.[20] We emphasize that this scheme does not ensure the positivity of density and the maximum principle for vapor quality of cell values. We recall that the original Roe scheme,[17] which requires satisfying the so-called Roe's condition (or, in other words, consistency with the integral form of the conservation law), only ensures positivity of density and mass fraction of vapor on a one-dimensional staggered grid (namely, fictitious cell $[x_i, x_{i+1}]$), whereas the exact Godunov scheme[7] enables preservation of $\rho \geq 0$, $1 \geq \alpha \geq 0$ on cell values because of the projection of the exact solution on the mesh.

C. Approximate Godunov Scheme: VFRoe Scheme with NCV

The original VFRoe scheme is an approximate Godunov scheme[7] that was first introduced in Refs. 15 and 16. The VFRoe-NCV scheme is a sequel of the latter that generalizes the approach by requiring some invertible change of variable, which provides the so-called NCV $Y(W)$. The scheme was introduced in Ref. 8, with applications to shallow water equations including comparison with the basic Godunov scheme (see Ref. 9) and applications to Euler gas-dynamics with arbitrary EOS in Ref. 10. Some possible extensions to the frame of nonconservative hyperbolic systems were defined and discussed in Refs. 11 and 12. Appendix D gives a description that permits straightforward coding of the scheme. A recent note[13] gives some detailed comparison of capacities of the scheme with comparison with the energy relaxation method,[37] the Rusanov scheme,[18] and Toro primitive variable Riemann solver (PVRS) scheme.[38] It also provides the main properties of the scheme when restricting to pure shock waves, steady or unsteady contact discontinuities, retaining simple EOS such as perfect gas EOS, Tamman EOS, or more sophisticated ones including stiffened gas EOS, Van der Waals EOS, Chemkin database, or tabulated laws (see Ref. 14). The field of practical applications of the VFRoe-NCV scheme up to now has mainly

concerned gas flows in turbines, in laminar and turbulent situations. We recall that fluxes are given by

$$\left(G_{i+\frac{1}{2}}^{\text{VFRoeNCV}}\right)^t = \left(0, 0, P_{i+\frac{1}{2}}^*, 0\right) \tag{26}$$

$$\boldsymbol{F}_{i+\frac{1}{2}}^{\text{VFRoeNCV}}(\tilde{\boldsymbol{W}}_i, \tilde{\boldsymbol{W}}_{i+1}) = \boldsymbol{F}\left[\boldsymbol{W}\left(Y_{i+\frac{1}{2}}^*\right)\right] \tag{27}$$

The starred value at interface $Y_{i+1/2}^*$ is obtained by solving a linear hyperbolic problem (see Appendix D). We only provide specific properties of the scheme when applying for $\boldsymbol{Y}^t = (\alpha, \tau, U, P)$ NCV. The first one concerns intermediate states of both pressure and velocity variables in the linearized Riemann solver at the interface. Denoting P_1 and P_2 (respectively, U_1 and U_2) values of pressure (respectively, velocity) on left side and right side of the contact discontinuity associated with eigenvalue U, one may easily check that (see Appendix D)

$$P_1 = P_2, \qquad U_1 = U_2$$

Moreover, we may check that

$$\alpha_1 = \alpha_i, \qquad \alpha_2 = \alpha_{i+1}$$

Thus, approximate values of the vapor quality at the interface predicted by VFRoe-NCV scheme are exact in the sense that they mimic the numerical values predicted by the exact Godunov scheme.[7] (The 1-wave and the 4-wave are ghost waves for vapor quality in the exact solution of the Riemann problem.) Obviously the maximum principle for the vapor quality holds true.

V. Numerical Results

System (1) admits solutions that may be discontinuous. Moreover, timescales associated with relaxation mass transfer terms and convective terms may be completely different; this may render computations rather tricky especially when the timescale associated with the relaxation term is small compared with the numerical time step imposed by the CFL condition in relation to convective effects. Fortunately, physical effects involved here are in favor of the fractional step method. Sudden variations of the cross section, for instance, when computing safety valves, may in addition penalize accuracy in some configurations. Extensive validation of VFRoe-NCV scheme has been previously performed when focusing on real gas flows and considering several EOS.[8–12] The efficiencies of the Rusanov scheme[18] and the approximate Roe-type[17] Riemann solver have been investigated in a different framework (Refs. 13 and 20). When restricting to Euler equations of gasdynamics with perfect gas EOS and focusing on the computation of shock tube experiments with a so-called first-order scheme, the rate of convergence (measuring error in L1 norm) is one-half for the concentration of pollutant (which does not vary in the genuinely nonlinear fields), and 1 for velocity and pressure (which do not change through the contact discontinuity). Figure 2 shows the evolution of the error for the concentration using either first-order or second-order schemes (in the latter case, the rate grows up to two-thirds). In all cases, the discrete error at time T is computed using a regular mesh according to

$$\|\phi - \phi_h\|(h, T) = \frac{\sum_{i=1}^{N} |\phi_h(x_i, T) - \phi(x_i, T)|}{\sum_{i=1}^{N} |\phi(x_i, T)|}$$

The rate of convergence for given value of CFL number is β provided that the error follows the law

$$\|\phi - \phi_h\|(h, T) = C(\phi, T)h^{\beta}$$

when h tends to 0. We restrict to the first-order version of the scheme in the sections that follow.

A. Steady Flow in a Nozzle Filled with Perfect Gas

The fluid is assumed to be represented by perfect gas EOS. Subsonic inlet and outlet boundary conditions are imposed so that a shock is present in the divergent part of the nozzle. Initial conditions are $P = 8$ bar, $T = 400$ K, $\alpha = 1$, and $U = 0$ m/s. Boundary conditions are $P_{\text{inlet}} = 10$ bar, $\alpha_{\text{inlet}} = 1$, $(\rho SU)_{\text{inlet}} = 1504$ kg/s, and $P_{\text{outlet}} = 8$ bar.

Figure 3 provides the rate of convergence of schemes toward the exact steady solution. We focus here on the mean pressure, the Mach number, and the mass flow rate. The rate of convergence is close to 1^- for all variables and for all schemes. Comparing Rusanov[18] and VFRoe[17] schemes, it appears that VFRoe provides the same accuracy using a mesh size h instead of $h/8$. Other examples are available in Ref. 29.

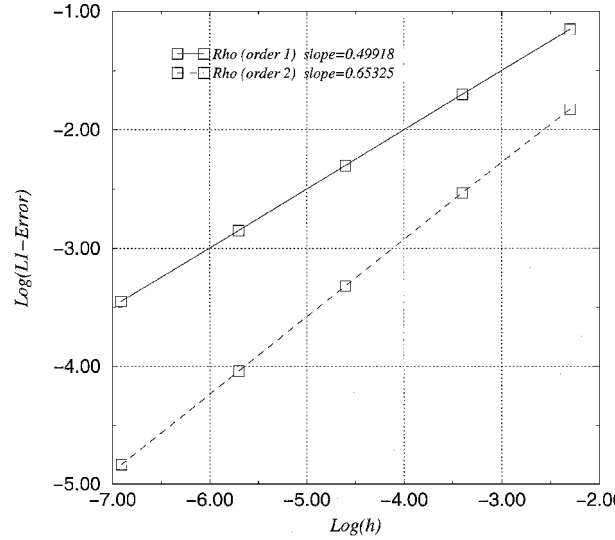

Fig. 2 L1 error norm when computing a pure contact discontinuity.

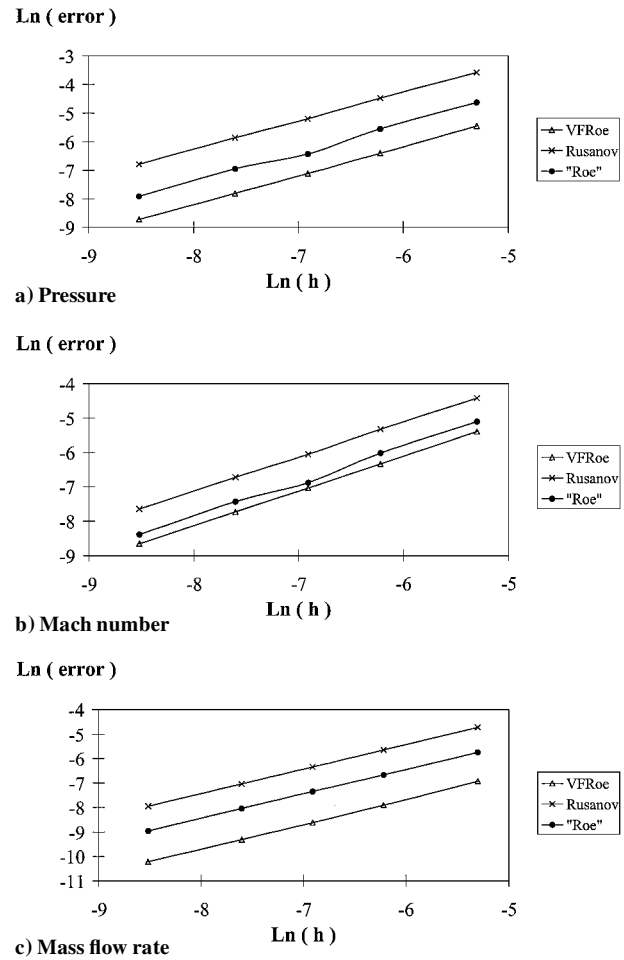

Fig. 3 Steady flow in a nozzle; L1 error norm.

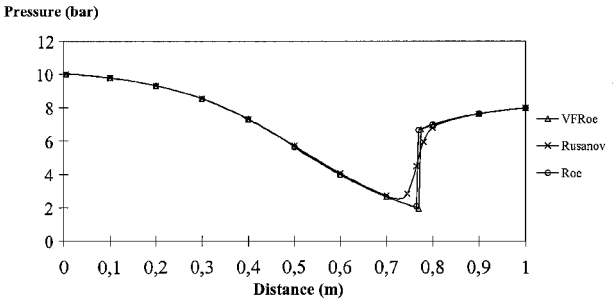

Pressure

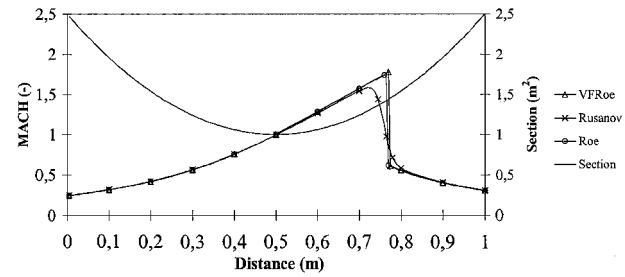

Mach number

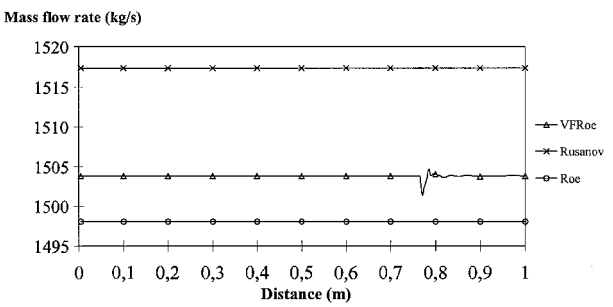

Mass flow rate

Fig. 4 Steady vapor flow in a nozzle (200 nodes).

B. Steady Flow in a Nozzle Filled with Real Gas

We use similar initial and boundary conditions but apply then for real gas EOS. Figure 4 shows that Rusanov scheme[18] does not provide a sharp (steady) shock profile in the divergent part when using a coarse mesh with 200 nodes. The numerical prediction of the steady mass flow rate (ρUS) is much better predicted when using the VFRoe scheme.[17] Note that we have plotted cell values of mass flow rate but not interface mass fluxes. Hence, the Roe scheme[17] and the Rusanov scheme[18] predict a slightly different value than expected. These discrepancies tend toward zero when the mesh is refined. The small glitch (which tends to 0 when the mesh is refined) around the shock location when using VFRoe scheme[17] is due to numerical perturbations coming from the subsonic outflow, which interact with the numerical shock profile; this is combined with the fact that the VFRoe-NCV scheme does not satisfy Roe's condition (or, in other words, consistency with the integral form of the conservation law) for complex EOS (see Refs. 8 and 10). We note, too, that the amplitude of this glitch is small compared with the difference between constant values predicted by the Roe and the Rusanov[18] schemes and expected value imposed by user at the inlet boundary. The relative error computed on the basis of the mass flow rate at interfaces predicted by the VFRoe scheme[17] (see Appendix D) is much lower than cell values of mass flow rate on given mesh size (which means that the flow is steady at a discrete point of view). Similar comments hold for cell values and interface values for the total enthalpy $H = (E + P)/\rho$. The most accurate prediction is given here by the VFRoe scheme.

C. SOD Shock Tube with Liquid Water

Shock tube tests simulate the solution of the Riemann problem with constant cross section $S(x) = S_0$. Thus, they are very useful to study the capabilities of schemes to compute transient flows. Physically speaking, they correspond to the following situation: a membrane, which initially separates two fluids with different thermodynamic states, is suddenly broken, so that waves start to propagate.

Initial conditions for the first shock tube test case are detailed next (subscripts L and R refer to the left-hand side and the right-hand side of the membrane):

$$P_L = 2000\ \text{bar}, \qquad \rho_L = 1017.8\ \text{kg/m}^3, \qquad \alpha_L = 1$$

$$u_L = 0\ \text{m/s}, \qquad P_R = 100\ \text{bar}, \qquad \rho_R = 838.3\ \text{kg/m}^3$$

$$\alpha_R = 1, \qquad u_R = 0\ \text{m/s}$$

Under these conditions, a shock wave travels to the right, followed by a contact discontinuity, whereas a rarefaction wave propagates to the left.

We have plot L1 error of predicted approximations provided by the three schemes using a CFL number 0.95 (Fig. 5). The measured rate of convergence is approximately the same for both velocity and pressure variables for both VFRoe-NCV and Roe-type[17] schemes: $\delta_U = \delta_P = 0.85$. It is, thus, close to the expected value of 1 (the second-order version of the scheme enables reaching rate 1^- on similar meshes). Part of the discrepancy is linked with that the EOS is complex so that some error around the contact discontinuity is introduced,[14] which slows down the convergence on these rather coarse meshes. Meanwhile the rate of convergence for the density is approximately $\delta_\rho = 0.65$ and, thus, still a bit greater than expected value of $\frac{1}{2}$ when h tends to 0. This is due to occurrence of variations of the density in the 1-rarefaction wave and through the 3-shock wave, which contribute to a balance between order $\frac{1}{2}$ and 1 on intermediate mesh sizes. This is confirmed by the measured rate of convergence of density for the Rusanov scheme,[18] which is approximately $\delta_\rho = 0.52$ instead of expected $\frac{1}{2}$. Actually, to reach the same accuracy, one needs almost twice the number of cells when using Rusanov scheme instead of Roe scheme[17] (or VFRoe scheme).

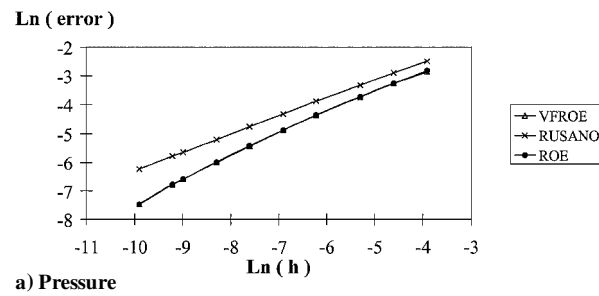

a) Pressure

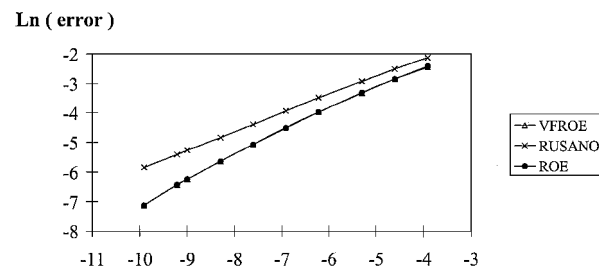

b) Velocity

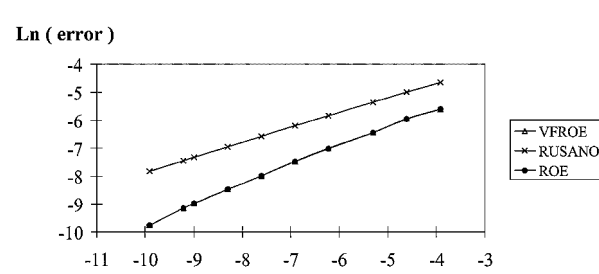

c) Density

Fig. 5 Shock tube filled with water; L1 error norm.

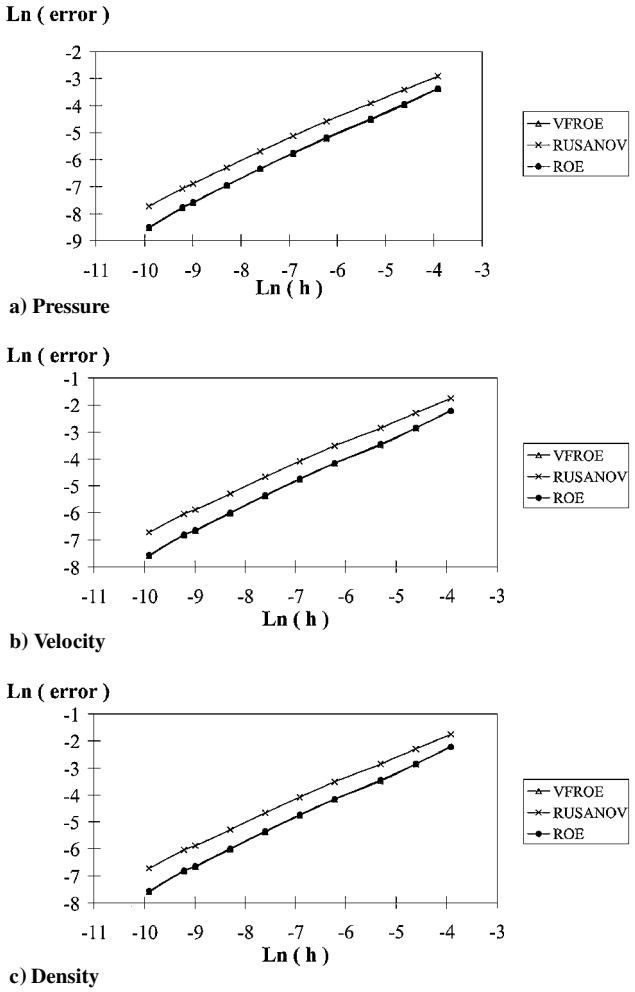

Fig. 6 Shock tube filled with vapor; L1 error norm.

D. SOD Shock Tube with Vapor

Initial conditions for the second shock tube tests case are

$$P_L = 5 \text{ bar}, \quad \rho_L = 2.215 \text{ kg/m}^3, \quad \alpha_L = 1, \quad u_L = 0 \text{ m/s}$$

$$P_R = 1 \text{ bar}, \quad \rho_R = 0.435 \text{ kg/m}^3, \quad \alpha_R = 1, \quad u_R = 0 \text{ m/s}$$

The CFL number is still 0.95. Similar comments hold here as in the preceding case (Fig. 6). Nonetheless, the performances for complex EOS around the contact discontinuity are better due to the behavior that in practice is very similar to the one associated with use of perfect gas EOS. The measured rate of convergence is still the same for both velocity and pressure for both VFRoe-NCV and Roe-type schemes[17] and is around $\delta_U = \delta_P = 0.9$, instead of expected value 1. The rate of convergence for the density is once more $\delta_\rho = 0.65$ (instead of $\frac{1}{2}$). There are indeed very few differences between rates of convergence of the three schemes here, but the Rusanov scheme[18] is still less accurate than the other two on a given mesh size.

E. Flashing Flow in a Nozzle

Initial conditions in the duct are

$$P = 15 \text{ bar}, \qquad T = 470 \text{ K}, \qquad \rho = 874.3 \text{ kg/m}^3$$

$$\alpha = 0, \qquad u = 0 \text{ m/s}$$

At the beginning of the computation, the pressure at the outflow suddenly decreases to

$$P_{\text{out}} = 10 \text{ bar}$$

The regular mesh contains 1000 nodes ($h = 10^{-3}$ m). The CFL number has been set to 0.9. Figure 7 shows the pressure distribution, the velocity distribution, and the void fraction distribution along the pipe

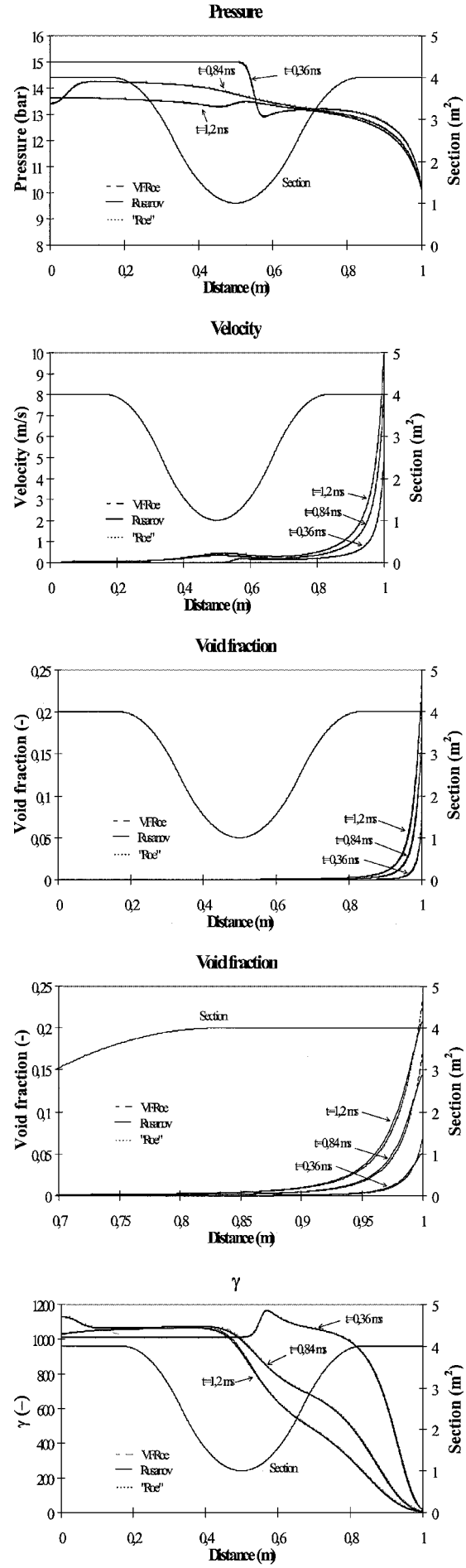

Fig. 7 Two-phase flashing flow.

due to rarefaction wave traveling to the left. Similar computations involving higher pressure ratios are reported in Ref. 27. The three schemes behave in a similar way, and there is indeed no contradiction with earlier results because no shock wave or contact discontinuity is present in the flowfield here, unlike in previous cases of unsteady shock tube experiments. Nonetheless, we may notice some differences between results close to the right boundary condition, where the vapor quality varies strongly.

VI. Conclusions

Several ways to compute unsteady flashing flows in variable cross section ducts have been summarized, on the basis of an approximate Godunov scheme[7] called VFRoe-NCV, an approximate form of Roe's scheme,[17] and the early Rusanov scheme.[18] All behave rather well; nonetheless, the Rusanov scheme suffers from a great amount of diffusion, which penalizes the scheme accuracy when computing steady or unsteady flows including shock waves. One of the main contributions concerns investigation of the true rate of convergence and of the level of accuracy for a given mesh size. Focusing on pressure and velocity variables (respectively, the density and the vapor quality), standard MUSCL-type extension combined with second-order Runge–Kutta time integration (which was not discussed herein) enables to reach first-order convergence rate on rather coarse, or industrial, meshes (respectively, rate of convergence of $\frac{2}{3}$), when computing unsteady shock tube experiments, and second-order when predicting regular flows.[9,10,13,27,29] The code is currently used in our company for practical purposes involving safety valves loaded with pressurized vapor or liquid.[27] The field of applications of the HRM is obviously rather wide in the industry. In all cases involving liquid water, or a mixture of vapor and liquid, it was noted that requiring sufficient small amount of error results in the use of very fine meshes, even in the one-dimensional framework. Actually, in some cases, a mesh with approximately 10,000 nodes may be compulsory; otherwise, coarser meshes may provide unrealistic predictions, which are not converged with respect to the mesh size.[27] Though not totally sufficient from a theoretical point of view, this is currently overcome using parallel versions of the code, which turns out to be a rough though efficient way to handle the situation.[26] All computations up to now have benefited from the fact that time scales associated with mass transfer terms and convective effects are in favor of the use of the fractional step technique. Some difficulties have nonetheless arisen in some cases when flashing phenomena occur close to some boundary condition. The strong coupling between nonlinear effects of convection and sources, but also on the nonlinear computation of local thermodynamic properties, renders the analysis of encountered slowdown of convergence cumbersome. The smearing of the slow contact discontinuity by upwinding schemes or, in other words, the poor accuracy around the latter linearly degenerate field, which in addition supports the jump of the vapor quality and of the mean density, may lead to nonlinear interactions in EOS and yield blow up of the code when the mesh is too coarse. Sometimes the only remedy is obtained by local refining of the mesh.

On the whole, the development and progress on algorithm improvements in at least three distinct directions are shown to still be mandatory. A first point concerns the treatment of contact discontinuities in conservative schemes using upwinding techniques, to minimize error around the latter, especially when complex EOS are involved. Several attempts in that direction have been already made (see Ref. 14 among others). A second problem is related to the different timescales associated with velocity of the fluid and the sound speed in almost incompressible fluids. This is indeed clearly related to the standard problem of preconditioning of compressible algorithms in flows with low-speed patterns. A third important point is connected with the coupling of source terms in convection dominated flows. This is particularly important in flows that may involve stiff source terms due to mass transfer. Progress has been made in that field, too (see Ref. 34 for instance), but it still deserves further study. Until now, three-dimensional computations of the HRM model with sufficiently fair accuracy have been almost beyond the reach of current computer facilities provided by local work stations.

Acknowledgments

Computational facilities have been provided by Electricité de France (EDF), Division Recherche Développement. The second author has benefited from financial support from EDF during his Ph.D. dissertation. The reviewers are acknowledged for their suggestions for changes, which helped improve the early version of the manuscript. The authors would like to thank Laurent Scliffet, who used to manage the MORSE project and encouraged these developments. We are also greatful to Thierry Gallouet for his continuous support and effort in helping us through encountered difficulties.

Appendix A: Discrete Maximum Principle for Vapor Quality

We examine here whether the maximum principle holds for the approximate values of the vapor quality, when using the Rusanov scheme. Focusing on mass conservation first, we get

$$\begin{aligned}\widehat{S}_i h_i \rho_i^{n+1} = \rho_i^n \Big(\widehat{S}_i h_i - (\Delta t/2) \Big\{ \widehat{S}_{i+\frac{1}{2}} \big[s\big(W_i^n, W_{i+1}^n\big) + U_i^n \big] \\ + \widehat{S}_{i-\frac{1}{2}} \big[s\big(W_{i-1}^n, W_i^n\big) - U_i^n \big] \Big\} \Big) \\ + (\Delta t/2) \big[s\big(W_i^n, W_{i+1}^n\big) - U_{i+1}^n \big] \widehat{S}_{i+\frac{1}{2}} \rho_{i+1}^n \\ + (\Delta t/2) \big[s\big(W_{i-1}^n, W_i^n\big) + U_{i-1}^n \big] \widehat{S}_{i-\frac{1}{2}} \rho_{i-1}^n \end{aligned} \tag{A1}$$

Thus, noting that

$$s\big(W_i^n, W_{i+1}^n\big) - U_{i+1}^n \geq 0, \qquad s\big(W_{i-1}^n, W_i^n\big) + U_{i-1}^n \geq 0 \tag{A2a}$$

$$s\big(W_i^n, W_{i+1}^n\big) + U_i^n \geq 0, \qquad s\big(W_{i-1}^n, W_i^n\big) - U_i^n \geq 0 \tag{A2b}$$

because of the definition of $s(W_i, W_{i+1})$ (maximum value of the spectral radius of Jacobian matrix on cell i and $i+1$), we immediately conclude that the mean density remains positive, for given positive values of the density at time t^n, provided that

$$\begin{aligned} 1 \geq (\Delta t/2h_i) \Big\{ \big(S_{i+\frac{1}{2}}/\widehat{S}_i\big) \big[s\big(W_i^n, W_{i+1}^n\big) + U_i^n \big] \\ + \big(S_{i-\frac{1}{2}}/\widehat{S}_i\big) \big[s\big(W_{i-1}^n, W_i^n\big) - U_i^n \big] \Big\} \end{aligned} \tag{A3}$$

Restricting to a constant cross section profile, the latter condition is the straightforward counterpart of the usual CFL condition:

$$1 \geq (\Delta t/h) \max_{\{i,i+1\}} \{(|U| + \hat{c})_i, (|U| + \hat{c})_{i+1}\}$$

If we turn now to the discrete values of the mass fraction of vapor, we note that

$$\begin{aligned}\widehat{S}_i h_i (\rho\alpha)_i^{n+1} = (\rho\alpha)_i^n \Big(\widehat{S}_i h_i - (\Delta t/2) \Big\{ S_{i+\frac{1}{2}} \big[s\big(W_i^n, W_{i+1}^n\big) + U_i^n \big] \\ + S_{i-\frac{1}{2}} \big[s\big(W_{i-1}^n, W_i^n\big) - U_i^n \big] \Big\} \Big) \\ + (\Delta t/2) \big[s\big(W_i^n, W_{i+1}^n\big) - U_{i+1}^n \big] S_{i+\frac{1}{2}} (\rho\alpha)_{i+1}^n \\ + (\Delta t/2) \big[s\big(W_{i-1}^n, W_i^n\big) + U_{i-1}^n \big] S_{i-\frac{1}{2}} (\rho\alpha)_{i-1}^n \end{aligned} \tag{A4}$$

Applying condition (A3), we may conclude that the mean vapor quality α remains positive. Also substracting Eq. (A1) from Eq. (A4), we get

$$\begin{aligned}\widehat{S}_i h_i [\rho(1-\alpha)]_i^{n+1} = [\rho(1-\alpha)]_i^n \Big(\widehat{S}_i h_i - (\Delta t/2) \Big\{ S_{i+\frac{1}{2}} \\ \times \big[s\big(W_i^n, W_{i+1}^n\big) + U_i^n \big] + S_{i-\frac{1}{2}} \big[s\big(W_{i-1}^n, W_i^n\big) - U_i^n \big] \Big\} \Big) \\ + (\Delta t/2) \big[s\big(W_i^n, W_{i+1}^n\big) - U_{i+1}^n \big] S_{i+\frac{1}{2}} [\rho(1-\alpha)]_{i+1}^n \\ + (\Delta t/2) \big[s\big(W_{i-1}^n, W_i^n\big) + U_{i-1}^n \big] S_{i-\frac{1}{2}} [\rho(1-\alpha)]_{i-1}^n \end{aligned} \tag{A5}$$

Hence, condition (A3) also implies that discrete values of $\rho(1\text{-}\alpha)$ remain positive, which completes the proof because discrete values of density are positive.

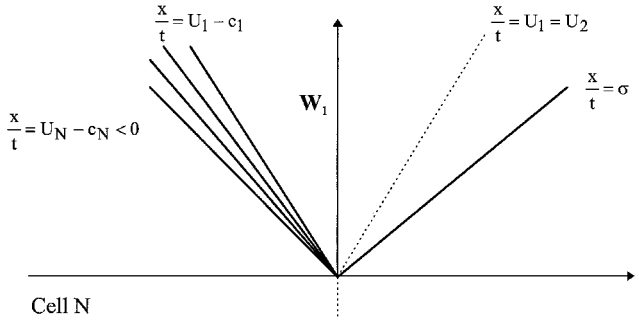

Fig. B1 Wave distribution at the outlet assuming subsonic flow.

Appendix B: Numerical Implementation of Subsonic Inflow and Outflow Boundary Conditions

Actually, the same method is applied in both cases, and, thus, we restrict here on the way to account for imposed pressure in a subsonic outflow. We assume subscript N refers to the last cell on the right of the computational domain and that the fluid flows to the right at the outlet. P_1 is set to be the imposed pressure level in the outlet section, and the unknowns are, thus, ρ_1, α_1, and U_1, which are the density, mass fraction of vapor, and mean velocity in the outlet section. These are simply determined assuming a 1-rarefaction wave (respectively, a one shock wave) connects state 1 with state N when P_N is greater than P_1 (respectively, when $P_N < P_1$). We focus on the first case, shown in Fig. B1.

Hence, preservation of the 1-Riemann invariants of the system gives

$$\alpha_1 = \alpha_N \tag{B1}$$

$$s(\rho_1, \alpha_1, P_1) = s(\rho_N, \alpha_N, P_N) \tag{B2}$$

$$U_1 = U_N + \int_{\rho_1}^{\rho_N} \frac{c(\rho, \alpha_N, s_N)}{\rho}\, \mathrm{d}\rho \tag{B3}$$

Relation (B2) provides unknown ρ_1 in a straightforward way because both P_1 and α_1 are given , due to Eq. (B1). Thus, one may compute the integral on the right-hand side of the last relation, which provides the last unknown U_1. In the opposite case, that is, when $P_N < P_1$, we use a 1-shock parametrization of curve:

$$\alpha_1 = \alpha_N \tag{B4}$$

$$U_1 = U_N - \left[[\rho]_1^N [P]_1^N (\rho_1 \rho_N)^{-1}\right]^{\frac{1}{2}} \tag{B5}$$

$$[e]_1^N \rho_1 \rho_N = [\rho]_1^N [(P_1 + P_N)/2] \tag{B6}$$

Obviously, in case of supersonic outflow, no condition should be imposed, and the state at the outlet interface simply is state N.

Appendix C: Formulas for Mass Transfer Term

If $P < 10$ bar

$$\theta = 6.51 \times 10^{-4} \alpha^{-0.257} \left[\frac{P_S(T_{\text{in}}) - P}{P_S(T_{\text{in}})}\right]^{-2.24}$$

Otherwise,

$$\theta = 3.84 \times 10^{-7} \alpha^{-0.54} \left[\frac{P_S(T_{\text{in}}) - P}{P_C - P_S(T_{\text{in}})}\right]^{-1.76}$$

In the preceding closures, $P_S(T_{\text{in}})$ is the saturated pressure corresponding to the inlet temperature and P_C is the thermodynamic critical pressure.

Appendix D: VFRoe-NCV Scheme with Nonconservative Variable $Y^t = (\alpha, \tau, U, P)$

We detail how to get starred value $\boldsymbol{W}(\boldsymbol{Y}^*)$. Starting from a uniform section, we rewrite locally at each cell interface the conservative system

$$\begin{aligned} &(\rho\alpha)_{,t} + (\rho\alpha U)_{,x} = 0, \qquad (\rho)_{,t} + (\rho U)_{,x} = 0 \\ &(\rho U)_{,t} + (\rho U^2)_{,x} + P_{,x} = 0, \qquad (E)_{,t} + [(E+P)U]_{,x} = 0 \end{aligned} \tag{D1}$$

in a straightforward counterpart (for regular solutions) as follows:

$$\begin{aligned} &(\alpha)_{,t} + U(\alpha)_{,x} = 0, \qquad (\tau)_{,t} + U(\tau)_{,x} - (\tau)(U)_{,x} = 0 \\ &(U)_{,t} + U(U)_{,x} + (\tau)P_{,x} = 0, \qquad (P)_{,t} + U(P)_{,x} + \hat{\gamma} P (U)_{,x} = 0 \end{aligned} \tag{D2}$$

Hence, linearizing around an average state at interface $(i + \frac{1}{2})$, we get

$$\boldsymbol{Y}_{,t} + \boldsymbol{C}[\boldsymbol{W}(\boldsymbol{Y}_i), \boldsymbol{W}(\boldsymbol{Y}_{i+1})]\boldsymbol{Y}_{,x} = 0$$

where

$$\boldsymbol{C}[\boldsymbol{W}(\boldsymbol{Y}_i), \boldsymbol{W}(\boldsymbol{Y}_{i+1})] = \begin{pmatrix} \bar{U} & 0 & 0 & 0 \\ 0 & \bar{U} & -\bar{\tau} & 0 \\ 0 & 0 & \bar{U} & \bar{\tau} \\ 0 & 0 & \bar{\gamma}\bar{P} & \bar{U} \end{pmatrix}_{i+\frac{1}{2}}$$

We denote $\boldsymbol{r}_k$ the basis of right eigenvectors of matrix $\boldsymbol{C}[\boldsymbol{W}(\boldsymbol{Y}_i), \boldsymbol{W}(\boldsymbol{Y}_{i+1})]$. We introduce the numerical sound velocity at each interface $(i + \frac{1}{2})$:

$$\hat{c}^2_{i+\frac{1}{2}} = \bar{\hat{\gamma}}_{i+\frac{1}{2}} \bar{P}_{i+\frac{1}{2}} \bar{\tau}_{i+\frac{1}{2}} \tag{D3}$$

where

$$\bar{\phi}_{i+\frac{1}{2}} = \tfrac{1}{2}(\phi_i + \phi_{i+1}) \tag{D4}$$

$\boldsymbol{W}^*_{i+\frac{1}{2}}$ is then given by

$$\begin{aligned} &\boldsymbol{W}^*_{i+\frac{1}{2}} = \boldsymbol{W}(\boldsymbol{Y}_i) \quad \text{if} \quad \bar{u}_{i+\frac{1}{2}} - \hat{c}_{i+\frac{1}{2}} > 0 \\ &\boldsymbol{W}^*_{i+\frac{1}{2}} = \boldsymbol{W}(\boldsymbol{Y}_1) \quad \text{if} \quad \bar{u}_{i+\frac{1}{2}} - \hat{c}_{i+\frac{1}{2}} < 0, \quad \bar{u}_{i+\frac{1}{2}} > 0 \\ &\boldsymbol{W}^*_{i+\frac{1}{2}} = \boldsymbol{W}(\boldsymbol{Y}_2) \quad \text{if} \quad \bar{u}_{i+\frac{1}{2}} < 0, \quad \bar{u}_{i+\frac{1}{2}} + \hat{c}_{i+\frac{1}{2}} > 0 \\ &\boldsymbol{W}^*_{i+\frac{1}{2}} = \boldsymbol{W}(\boldsymbol{Y}_{i+1}) \quad \text{if} \quad \bar{u}_{i+\frac{1}{2}} + \hat{c}_{i+\frac{1}{2}} < 0 \end{aligned} \tag{D5}$$

$\boldsymbol{Y}_1$ and $\boldsymbol{Y}_2$ are two intermediate states arising when solving the linear hyperbolic problem:

$$\boldsymbol{Y}_1 = \boldsymbol{Y}_i + (\alpha_1)_{i+\frac{1}{2}} \hat{\boldsymbol{r}}_1 \tag{D6a}$$

$$\boldsymbol{Y}_2 = \boldsymbol{Y}_{i+1} - (\alpha_4)_{i+\frac{1}{2}} \hat{\boldsymbol{r}}_4 \tag{D6b}$$

with

$$\hat{\boldsymbol{r}}^t_1 = \left(0, \bar{\tau}_{i+\frac{1}{2}}, \hat{c}_{i+\frac{1}{2}}, -\bar{\hat{\gamma}}_{i+\frac{1}{2}} \bar{P}_{i+\frac{1}{2}}\right) \tag{D7a}$$

$$\hat{\boldsymbol{r}}^t_2 = (1, 0, 0, 0) \tag{D7b}$$

$$\hat{\boldsymbol{r}}^t_3 = (0, 1, 0, 0) \tag{D7c}$$

$$\hat{\boldsymbol{r}}^t_4 = \left(0, \bar{\tau}_{i+\frac{1}{2}}, -\hat{c}_{i+\frac{1}{2}}, -\bar{\hat{\gamma}}_{i+\frac{1}{2}} \bar{P}_{i+\frac{1}{2}}\right) \tag{D7d}$$

See Fig. D1.

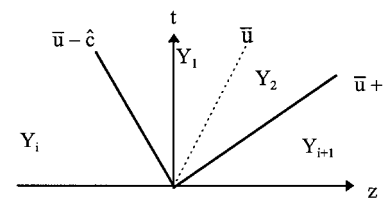

Fig. D1 Linearized Riemann problem.

The coefficients read

$$(\alpha_1)_{i+\frac{1}{2}} = \frac{1}{2}\left[\frac{u_{i+1}-u_i}{\hat{c}_{i+\frac{1}{2}}} - \frac{\bar{\tau}_{i+\frac{1}{2}}}{\hat{c}^2_{i+\frac{1}{2}}}(P_{i+1}-P_i)\right] \quad \text{(D8a)}$$

$$(\alpha_4)_{i+\frac{1}{2}} = -\frac{1}{2}\left[\frac{u_{i+1}-u_i}{\hat{c}_{i+\frac{1}{2}}} + \frac{\bar{\tau}_{i+\frac{1}{2}}}{\hat{c}^2_{i+\frac{1}{2}}}(P_{i+1}-P_i)\right] \quad \text{(D8b)}$$

Coefficients are obtained by solving

$$\boldsymbol{Y}_{i+1} = \boldsymbol{Y}_i + \sum_{k=1}^{4}(\alpha_k)_{i+\frac{1}{2}}\hat{\boldsymbol{r}}_k$$

An entropy correction at sonic points in rarefaction waves is required as usual. Because of the previous decomposition, one may easily see that the numerical intermediate states are in agreement with exact intermediate states because $P_1 = P_2$ and $U_1 = U_2$. Moreover, we check that $\alpha_1 = \alpha_i$ and $\alpha_2 = \alpha_{i+1}$.

References

[1]Bolle, L., Downar-Zapolski, P., Franco, J., and Seynhaeve, J. M., "Experimental and Theoretical Analysis of Flashing Water Through a Safety Valve," International Symposium on Heat and Mass Transfer in Chemical Process Industry Accidents, Rome, Sept. 1994.

[2]Bilicki, Z., and Kardas, D., "Approximation of Thermodynamic Properties for Subcooled Water and Superheated Steam," Inst. for Fluid Flow Machinery, Polish Academy of Sciences, Nr. Arch. 185/91, Gdansk, Poland, 1991.

[3]Bilicki, Z., Kestin, J., and Pratt, M. M., "A Reinterpretation of the Results of the Moby-Dick Experiments in Terms of the Nonequilibrium Model," *Journal of Fluids Engineering*, Vol. 112, 1990, pp. 212–217.

[4]Downar-Zapolski, P., Bilicki, Z., Bolle, L., and Franco, J., "The Non-Equilibrium Model for One-Dimensional Flashing Liquid Flow," *International Journal of Multiphase Flow*, Vol. 22, 1996, pp. 473–483.

[5]Faucher, E., Herard, J. M., Barret, M., and Toulemonde, C., "Computation of Flashing Flows in Variable Cross Section Ducts," *International Journal of Computational Fluid Dynamics*, Vol. 13, No. 3, 2000, pp. 365–391.

[6]Eymard, R., Gallouët, T., and Herbin, R., "Finite Volume Methods," *Handbook for Numerical Analysis*, edited by P. G. Ciarlet and J. L. Lions, Vol. 7, North-Holland, Amsterdam, 2000, pp. 729–1020.

[7]Godunov, S. K., "A Finite Difference Method for the Numerical Computation of Discontinuous Solutions of the Equations of Fluid Dynamics," *Matematicheskii Sbornik*, Vol. 47, 1959, pp. 217–300.

[8]Buffard, T., Gallouët, T., and Hérard, J. M., "Schéma VFRoe en Variables Caractéristiques. Principe de Base et Application aux Gaz Réels," Div. Recherche Développement, Electricite de France, EDF Rept. HE-41/96/041/A, Chatou, France, 1996 (in French).

[9]Buffard, T., Gallouët, T., and Hérard, J. M., "A Naive Scheme to Solve Shallow Water Equations," *Comptes Rendus Académie des Sciences Paris*, Vol. 326, Série 1, 1998, pp. 385–390.

[10]Buffard, T., Gallouët, T., and Hérard, J. M., "A Sequel to a Rough Godunov Scheme. Application to Real Gases," *Computers and Fluids*, Vol. 29, No. 7, 2000, pp. 813–847.

[11]Buffard, T., Gallouët, T., and Hérard, J. M., "A Naive Riemann Solver to Compute a Non Conservative Hyperbolic System," *International Series on Numerical Mathematics*, Vol. 129, 1999, pp. 129–138.

[12]Buffard, T., Gallouët, T., and Hérard, J. M., "An Approximate Godunov Scheme to Compute Turbulent Real Gas Flow Models," AIAA paper 99-3349, 1999.

[13]Gallouët, T., Herard, J. M., and Seguin, N., "Some Recent Finite Volume Schemes to Compute Euler Equations Using Real Gas EOS," Centre de Mathématique et d'Informatique, Laboratoire Analyse Topologie Probabilités, Preprint LATP 00-021, Univ. de Provence, Marseille, France, 2000.

[14]Gallouët, T., Herard, J. M., and Seguin, N., "An Hybrid Scheme to Compute Contact Discontinuities in Euler Systems," Div. Recherche Développement, Electricite de France, Internal EDF Rept. HI-81/01/011/A, Chatou, France, 2001.

[15]Gallouët, T., and Masella, J. M., "A Rough Godunov Scheme," *Comptes Rendus Académie des Sciences Paris*, Vol. 323, Série 1, 1996, pp. 77–84.

[16]Masella, J. M., Faille, I., and Gallouët, T., "On a Rough Godunov Scheme," *International Journal of Computational Fluid Dynamics*, Vol. 12, 1999, pp. 133–149.

[17]Roe, P. L., "Approximate Riemann Solvers, Parameter Vectors and Difference Schemes," *Journal of Computational Physics*, Vol. 43, 1981, pp. 357–372.

[18]Rusanov, V. V., "The Calculation of the Interaction of Non-Stationary Shock Waves and Obstacles," *Zhurnal Vich. Nat.*, No. 2, 1961, pp. 304–320.

[19]Einfeldt, B., Munz, C. D., Roe, P. L., and Sjogreen, B., "On Godunov Type Methods Near Low Densities," *Journal of Computational Physics*, Vol. 92, No. 2, 1991, pp. 273–295.

[20]Brun, G., Hérard, J. M., Jeandel, D., and Uhlmann, M., "An Approximate Roe-Type Riemann Solver for a Class of Realizable Second Order Closures," *Journal of Computational Physics*, Vol. 151, No. 2, 1999, pp. 990–996.

[21]Combe, L., and Hérard, J. M., "A Finite Volume Algorithm to Compute Dense Compressible Gas–Solid flows," *AIAA Journal*, Vol. 37, No. 3, 1999, pp. 335–342.

[22]Declercq, E., Forestier, A., Hérard, J. M., Louis, X., and Poissant, G., "An Exact Riemann Solver for a Multicomponent Turbulent Flow," *International Journal of Computational Fluid Dynamics*, Vol. 14, 2001, pp. 117–131.

[23]Herard, J. M., "Solveur de Riemann approché pour un système hyperbolique non conservatif issu de la turbulence compressible," Div. Recherche Développement, Electricite de France, EDF Rept. HE-41/95/009/A, Chatou, France, 1995 (in French).

[24]Dal Maso, G., Le Floch, P. G., and Murat, F., "Definition and Weak Stability of Non Conservative Products," *Journal de Mathématiques Pures et Appliquées*, Vol. 74, 1995, pp. 483–548.

[25]Le Floch, P. G., "Entropy Weak Solutions to Non Linear Hyperbolic Systems in Non Conservative Form," *Communications in Partial Differential Equations*, Vol. 13, No. 6, 1996, pp. 669–727.

[26]Berthou, J. Y., and Fayolle, E., "Parallélisation de la Version Industrielle du Code HRM1D: ECOSS," Div. Recherche Développement, Electricite de France, EDF Rept. HI-76/00/016/A, Chatou, France, 2000.

[27]Faucher, E., Herard, J. M., Levu, G., and Scliffet, L., "Simulation Numérique d'Écoulements Diphasiques Eau-Vapeur. Application à l'APRP et à Quelques Problèmes de Fonctionnement de Soupape," Div. Recherche Développement, Electricite de France, Internal EDF Rept. HE-41/99/037/A, Chatou, France, 1999 (in French).

[28]Dubois, F., "Boundary Conditions and the Osher Scheme for the Euler Equations of Gas Dynamics," Centre de Mathématiques Appliquées de l'Ecole Polytechnique, CMAP Rept. 170, Palaiseau, France, 1987.

[29]Faucher, E., "Simulation numérique d'écoulements unidimensionnels instationnaires avec auto vaporisation," Ph.D. Dissertation, Institut Universitaire de Technologie Melun Sénart, Lieusaint, France, Jan. 2000.

[30]Lemaire, C., "Caractérisation et Modélisation du Blocage de Débit en Écoulement Dispersé à Deux Constituants en Géométrie Tridimensionnelle," Ph.D. Dissertation, Université Joseph Fourier, Grenoble, France, Nov. 1999.

[31]Lemaire, C., Lemonnier, H., and Dehais, G., "Determination of Two-Phase Critical Flow: Implementation and Assessment of a Reference Technique," 36th European Two-Phase Flow Group Meeting, 1st European-Japanese Two-Phase Flow Group Meeting, Portoroz, Slovenia, June 1998.

[32]Pollack, R., "Die thermodynamischen Eigenschaften von Wasser dargestellet durch eine Kanonische Zustands Gleichung fur die Fluiden Homogenen and Heterogenen Zustande bis 1200 Kelvin und 3000 Bars," Ph.D. Dissertation, Ruhr Univ., Germany, 1974.

[33]Baraille, R., Bourdin, G., Dubois, F., and Leroux, A. Y., "Une Version à Pas Fractionnaires du Schéma de Godunov pour l'Hydrodynamique," *Comptes Rendus Académie des Sciences Paris*, Vol. 314, Série 1, 1992, pp. 147–152.

[34]Papalexandris, M. V., Leonard, A., and Dimotakis, P. E., "Unsplit Schemes for Hyperbolic Conservation Laws with Source Terms in One Space Dimension," *Journal of Computational Physics*, Vol. 134, 1997, pp. 31–61.

[35]Smoller, J., *Shock Waves and Reaction–Diffusion Equations*, Springer-Verlag, Berlin, 1983.

[36]Godlewski, E., and Raviart, P. A., *Numerical Analysis for Hyperbolic Systems of Conservation Laws,* Springer-Verlag, Berlin, 1997.

[37]In, A., "Numerical Evaluation of an Energy Relaxation Method for Inviscid Real Fluids," *SIAM Journal of Scientific Computing*, Vol. 21, No. 1, 1999, pp. 340–365.

[38]Toro, E. F., *Riemann Solvers and Numerical Methods for Fluid Dynamics,* Springer-Verlag, Berlin, 1997.

J. R. Bellan
Associate Editor